Contents lists available at ScienceDirect

Journal of Molecular Spectroscopy
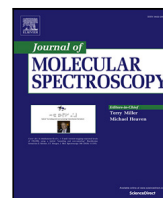
Infrared free-electron laser irradiation of carbon dioxide ice

Sergio Ioppolo [a,*], Jennifer A. Noble [b,c], Alejandra Traspas Muiña [a], Herma M. Cuppen [d], Stéphane Coussan [b], Britta Redlich [e]

[a] School of Electronic Engineering and Computer Science, Queen Mary University of London, London E1 4NS, UK
[b] CNRS, Aix-Marseille Univ, PIIM, Marseille 13397, France
[c] School of Physical Sciences, University of Kent, Canterbury CT2 7NH, UK
[d] Radboud University, Institute for Molecules and Materials, Nijmegen 6525 AJ, The Netherlands
[e] FELIX Laboratory, Radboud University, Nijmegen 6525 ED, The Netherlands

ARTICLE INFO

ABSTRACT

Interstellar ice grains are believed to play a key role in the formation of many of the simple and complex organic species detected in space. However, many fundamental questions on the physicochemical processes linked to the formation and survival of species in ice grains remain unanswered. Field work at large-scale facilities such as free-electron lasers (FELs) can aid the investigation of the composition and morphology of ice grains by providing novel tools to the laboratory astrophysics community. We combined the high tunability, wide infrared spectral range and intensity of the FEL beam line FELIX-2 at the HFML-FELIX Laboratory in The Netherlands with the characteristics of the ultrahigh vacuum LISA end station to perform wavelength-dependent mid-IR irradiation experiments of space-relevant pure carbon dioxide (CO_2) ice at 20 K. We used the intense monochromatic radiation of FELIX to inject vibrational energy at selected frequencies into the CO_2 ice to study ice restructuring effects *in situ* by Fourier Transform Reflection–Absorption Infrared (FT-RAIR) spectroscopy. This work improves our understanding of how vibrational energy introduced by external triggers such as photons, electrons, cosmic rays, and thermal heating coming from a nascent protostar or field stars is dissipated in an interstellar icy dust grain in space. Moreover, it adds to the current literature debate concerning the amorphous and polycrystalline structure of CO_2 ice observed upon deposition at low temperatures, showing that, under our experimental conditions, CO_2 ice presents amorphous characteristics when deposited at 20 K and is unambiguously crystalline if deposited at 75 K.

1. Introduction

To date, more than 240 different species have been identified in space in the gas phase [1]. Since gas-phase reaction rates are often found to be too low to account for the observed abundances of species in space, the icy mantles of interstellar dust grains are believed to give rise to a rich prebiotic chemistry, which feeds complex organic molecules (COMs) to star-forming regions and ultimately to planetary systems [2–4]. Current infrared (IR) observations show that laboratory spectral data on peak position and feature width can be used to extract information on layering and mixing of interstellar ices [5,6]. The NASA James Webb Space Telescope (JWST) mission will enable the observation of interstellar ices over a wide wavelength range (0.6–28.3 μm) toward a large variety of sources. Its high spectral resolution will allow the observation of spectral characteristics depending on different ice morphologies, thermal histories, and mixing environments in star-forming regions, beyond simply measuring feature width and peak

position. However, the large amount of new observational data that will be provided by JWST can only be correctly interpreted if a parallel effort is made in laboratories to develop new experimental methodologies, for instance, at free-electron laser (FEL) large-scale facilities, to provide unprecedented spectroscopic details on morphologies and dynamics within interstellar ice analogs.

Believed to be largely amorphous in nature, the structure of interstellar ices is still under investigation. In space, dust grains covered in icy material are continuously exposed to 'energetic' particles such as cosmic rays, electrons, and UV photons that release excess energy into the ice target causing physicochemical changes within the grain mantle. Exothermic surface chemical reactions induced by gas-phase species landing on the grain surface can also affect the structure and dynamics within interstellar ices. Understanding how exothermic chemical reactions deposit large amounts of energy into icy mantles covering dust grains containing some of the molecular building blocks for life,

---

could help explain the formation of prebiotic compounds in space. Particularly, surface chemical reactions can be broken down into various elementary processes, namely, adsorption, diffusion, dissociation, product formation, energy dissipation, and desorption. The mechanisms underlying energy dissipation at the atomic scale thus decide the fate of possible subsequent processes.

To date, little is known about how the energy released into an icy grain after a surface reaction or cosmic ray interaction dissipates within the grain [7]. Direct experimental quantification of energy dissipation by time-resolved techniques with concurrent atomic resolution is still an ongoing challenge [8,9]. Moreover, the effect of low energy photon irradiation, *i.e.*, in the infrared regime, on – for instance – the hydrogen bonding network of water ice has been scarcely addressed. Only a couple of IR irradiation studies have been performed on crystalline water ice at elevated temperatures, the main purpose of which was to investigate desorption efficiencies and products [10,11]. In terms of porous amorphous solid water (pASW), some of us have previously studied the pASW surface via the 'dangling' OH stretching modes [12–14], revealing an irreversible restructuring of these surface modes upon selective IR irradiation by means of a table-top pulsed optical parametric oscillator (OPO) laser. Our recent combined laboratory and theoretical work on selective FEL irradiation of pASW showed that ices can absorb vibrational energy in the broad IR (4000–400 cm^{-1}, 2.5–25 μm) and terahertz (THz, 0.1–10 THz, 30–3000 μm) spectral ranges, causing local heating within the ice structure and at the surface that leads to a reorganization of the ice toward a more ordered material [15].

Selective IR/THz experiments at FEL facilities are needed to better understand the nature of IR/THz modes in solids as well as to time-resolve dynamics and energy relaxation processes within condensed matter. Particularly important to the fields of astrochemistry, astrobiology, surface science, and catalysis are physicochemical studies of diffusion, segregation, reaction, and ultimately desorption of molecules at the surface and in the bulk of space-relevant ice layers. Here, we present the first laboratory selective FEL irradiation study of pure solid amorphous and crystalline carbon dioxide (CO_2) ices at 20 K. Based on our previous work on ASW, cubic ice (Ic), and hexagonal ice (Ih), we selected CO_2 as our target for the following reasons. ASW is the most abundant form of ice in the Universe and provides the surface upon, and matrix within which, volatile species react to form prebiotic molecules, as well as absorbing some of the excess reaction energy [13,16]. After H_2O, CO_2 is one of the most abundant solid-phase species in the interstellar medium (ISM), with abundances of between 20 and 30% that of H_2O ice, depending on the object observed [6]. In dense molecular clouds, CO_2 is formed in the solid phase primarily through the CO+OH surface reaction [17–20]. Therefore, CO_2 tends to reside mostly in a H_2O-rich layer, where OH radicals are more abundant and available for reaction with CO molecules. Additionally, CO_2 and more complex species form in mixed ices that undergo 'energetic' processing such as thermal heating, photon, electron, and ion irradiation that dramatically affect the bulk and surface structure of the ice [21–29]. Therefore, understanding changes induced upon chemical or physical perturbation in CO_2 ices is pivotal to unraveling molecular evolution in space.

Finally, there is an ongoing debate in the literature on the structure of deposited CO_2 ice under laboratory conditions and its corresponding spectroscopic fingerprint assignments that can help interpreting present and future observations of CO_2 ice in space [30–36]. This work adds to the scientific discussion on the topic by providing new independent evidence of the morphology of CO_2 ice deposited at different temperatures with implications for the ISM and the Solar System.

2. Experimental methods

Experiments are carried out using the laboratory ice surface astrophysics (LISA) ultrahigh vacuum (UHV) end station at the HFML-FELIX Laboratory, Radboud University, The Netherlands. Details of the experimental setup are given in the Supporting Material. Here we discuss the experimental methodology used during a standard experiment. Briefly, pure CO_2 ices are grown on the gold substrate of the main chamber at temperatures of 20 and 75 K. Carbon dioxide (99.995% CO_2, CANgas) is used as received from Sigma-Aldrich. Firstly, a few mbar of CO_2 gas are introduced in the dosing line, while monitoring the pressure mass-independently. Then, gases are admitted into the main chamber by a manual all-metal needle valve. During deposition, the pressure in the main chamber is measured by means of the cold cathode gauge and the QMS and it is kept constant at 1×10^{-6} mbar by adjusting the aperture of the all-metal inlet valve. QMS calibration experiments are performed at room temperature to find a correlation between residual mass signals detected with the cryostat on and off.

At the beginning of a standard experiment, the cryostat is turned on, the MCT detector is filled with liquid nitrogen, and the nitrogen purge is activated. Once the base temperature of the substrate is reached in a matter of a few hours, the gold substrate is flash heated to 200 K to further clean its surface prior to gas deposition. Then, upon reaching the selected substrate temperature (20 or 75 K), a background FTIR spectrum comprising 512 co-added scans with a resolution of 0.5 cm^{-1} is acquired in the 4000–600 cm^{-1} range to remove any signal along the IR beam path that does not arise from the ice sample. During deposition, FTIR spectra with 8 co-added scans are acquired every 20 s to monitor the ice growth, while residual gas is measured by the QMS. At the end of all depositions, an FTIR spectrum with 256 co-added scans is acquired. If the deposition temperature is not 20 K, the ice is then cooled and kept at this temperature and another FTIR spectrum with 256 co-added scans is acquired prior to any exposure to FEL radiation. All spectra are acquired at a resolution of 0.5 cm^{-1}. Fig. 1 shows the FT-RAIR spectra of pure CO_2 deposited at 20 K and at 75 K and then cooled to 20 K. The figure highlights the overtone ($\nu_1 + \nu_3$ at 3708 cm^{-1} and $2\nu_2 + \nu_3$ at 3599 cm^{-1}), stretching (ν_3 at 2376 cm^{-1}), and bending (ν_2 at 675 cm^{-1}) modes of pure $^{12}CO_2$ as well as the natural presence of $^{13}CO_2$ (ν_3 at 2283 cm^{-1}) in the deposited sample. Differences in spectral profiles and absorption peak positions compared to some literature values are due to the fact that here spectra are acquired by means of RAIR spectroscopy as opposed to transmission spectroscopy [32,34].

The molecular column density C (molecules cm^{-2}) of the deposited CO_2 ices at both 20 and 75 K is calculated by integrating a modified Beer–Lambert Equation (Eq. (1)) to account for the RAIR mode configuration over the ν_3 absorbance band of CO_2:

$$C = \ln(10)\frac{\sin(\theta)}{2A'(\nu)} \int \tau(\nu)d\nu, \qquad (1)$$

where $A'(\nu)$ is the integrated band strength, $\tau(\nu)$ is the optical depth (cm^{-1}), and θ is the FTIR incident angle of 13°. Based on the work of Gerakines and Hudson [32], we chose $A'(\nu_3) = 1.18 \times 10^{-16}$ cm molecule^{-1} and $A'(\nu_3) = 7.6 \times 10^{-17}$ cm molecule^{-1} as the integrated band strengths for pure CO_2 deposited at 20 K and at 75 K and then cooled to 20 K, respectively [32,37,38]. In our experiments, the column densities of CO_2 deposited at 20 and at 75 K are 11×10^{15} and 17×10^{15} molecule cm^{-2}, respectively. Apart from the deposition temperature, all other parameters are kept the same during deposition, *e.g.*, deposition time (~190 s) and residual pressure in the main chamber (1×10^{-6} mbar). Once calculated, the column densities are used to determine the ice thicknesses in nm as per Eq. (2):

$$d = \frac{CZ}{\rho N_A} \times 10^7, \qquad (2)$$

where Z is the molecular mass of the CO_2 molecule (g mol^{-1}), ρ is the density of the ice, which we have taken to be 1.2 g cm^{-3} and 1.67 g cm^{-3} for CO_2 deposited at 20 K and at 75 K, respectively [39], and N_A is the Avogadro constant (6.02×10^{23} molecule mol^{-1}). Hence, we estimate pure CO_2 deposited at 20 and 75 K to be both ~7 nm thick with a deposition rate of ~0.037 nm s^{-1}.
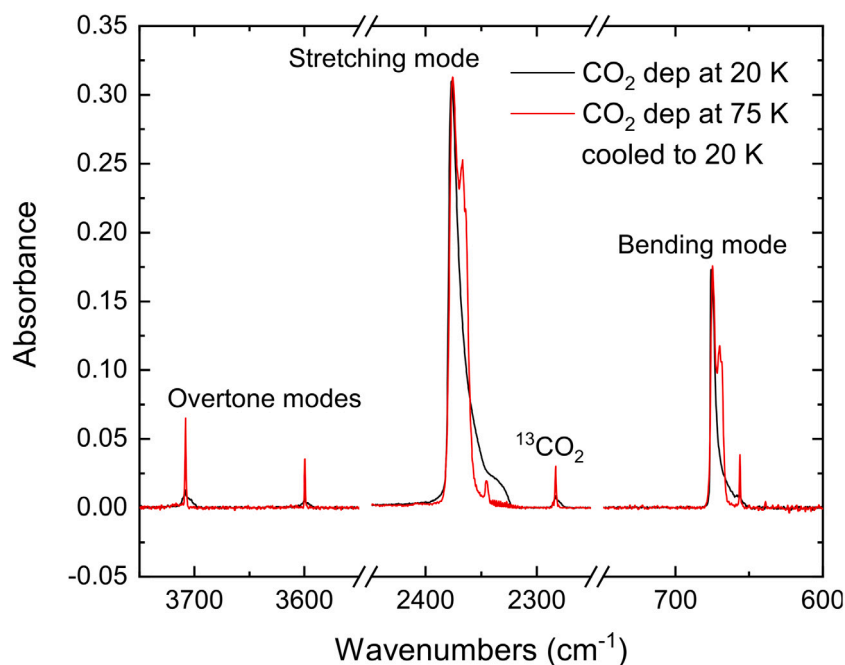
Fig. 1. FT-RAIR spectra of pure CO_2 deposited at 20 K (black solid line) and at 75 K and then cooled to 20 K (red solid line) marked with absorption modes in the MIR. Solid $^{13}CO_2$ is also visible.

Table 1
Experimental details of CO_2 ice exposed to FEL radiation.

Molecule	Deposition T K	FEL irradiation μm	TPD K min^{-1}
CO_2	20	3.2, 4.19, 4.21, 4.22, 4.28, 14.76, 15.18	2.5
CO_2	20	–	2.5
CO_2	75	3.2, 4.2, 4.22, 4.25, 14.8	–

Ices are irradiated at 20 K using the FELIX-2 infrared FEL source with macropulses of 5 Hz repetition rate and at frequencies in the MIR range (3.2–15.2 μm). All irradiations of pure CO_2 ice deposited at 20 K and at 75 K are carried out for five minutes to ensure the complete saturation of any structural changes in the ice. The spectral FWHM of the FELIX beam is on the order of 0.8% $\delta\lambda/\lambda$ for all wavelengths. Unless otherwise specified, the laser macropulse energy at longer wavelengths (~130 mJ in the 15 μm wavelength region) is attenuated to ~20 mJ to match that in the 3–4 μm region. Thus, at all wavelengths investigated, the average power is ~0.03 W, with a laser fluence at the sample of approximately ~0.2 J/cm^2. Table 1 shows the main experiments and their FEL irradiation details.

FTIR spectra are acquired before and after irradiation, from which difference spectra are obtained to highlight changes in the IR band profiles. All data analysis and spectral manipulation is performed using *in house* python scripts. Unless specified, FEL irradiations are performed on unirradiated ice. During FEL irradiation, the QMS is used to monitor any possible desorption of species from the ice. Upon completion of FEL irradiations, a TPD experiment is usually performed by means of the QMS as well as the FTIR with spectra of 128 co-added scans collected every 120 s. Since a heating ramp of 2.5 K min^{-1} is used, each FTIR spectrum is acquired every 5 K from 20 to 200 K. A TPD control experiment of a CO_2 ice deposited at 20 K and not exposed to FEL irradiation is performed for comparison and interpretation of the FEL exposure experiments.

3. Results and discussion

3.1. FEL irradiation of CO_2 ice deposited at 20 K

The left panels of Fig. 2 show an FT-RAIR spectrum of pure CO_2 ice deposited at 20 K in the v_3 and v_2 spectral ranges (upper and lower panels, respectively). Both v_3 and v_2 modes exhibit transverse optical (TO) and longitudinal optical (LO) phonons in which the normal vibrations propagate through the ice lattice perpendicular and parallel to the direction of the IR field, respectively. In our FT-RAIR spectra, the LO phonons at 4.2 and 14.8 μm are stronger than the TO phonons at 4.27 and 15.2 μm for the v_3 and v_2 modes, respectively [30,40,41]. Colored arrows indicate the frequencies at which the ice has been exposed to FELIX-2 radiation for five minutes of continuous exposure at a time and always on fresh, unirradiated ice spots. Here and throughout the rest of the paper, we will use the same color scheme. Vertical color-coded strips indicate the spectral FWHM of the FELIX beam at each selected wavelength. Around the peak of the v_3 mode, the spectral FWHM of the FELIX beam is such that at all three selected FEL irradiation frequencies the three irradiations overlap with one other. This can explain the similar effects seen in the ice after FEL exposure for the three irradiations at 4.19, 4.21, and 4.22 μm by comparing FT-RAIR spectra before and after FEL exposure (upper-right panel of Fig. 2). Such difference spectra reveal that the ice has undergone a degree of restructuring as well as perhaps some desorption. The latter is highlighted by the fact that, upon exposure to FEL radiation, both v_3 and v_2 modes decreased in intensity, as shown by the negative peaks in the upper three difference spectra of the upper-right panel of Fig. 2. Moreover, the v_3 and v_2 band shapes present modified profiles suggesting restructuring of the ice, as shown by the positive peaks in the three difference spectra. More pronounced negative peaks are observed for irradiations around the LO phonon mode peak of the v_3 band. The fourth FEL irradiation at 4.28 μm on the red wing (*i.e.*, TO phonon) of the CO_2 stretching mode presents only weaker negative peaks. FEL irradiation can depend on the absorption cross section of the v_3 band, showing weaker effects at 4.28 μm. Moreover, a larger restructuring effect seen after FEL irradiations of the LO versus the TO phonon modes of the v_3 band can be explained by the fact that the FELIX-2 optical
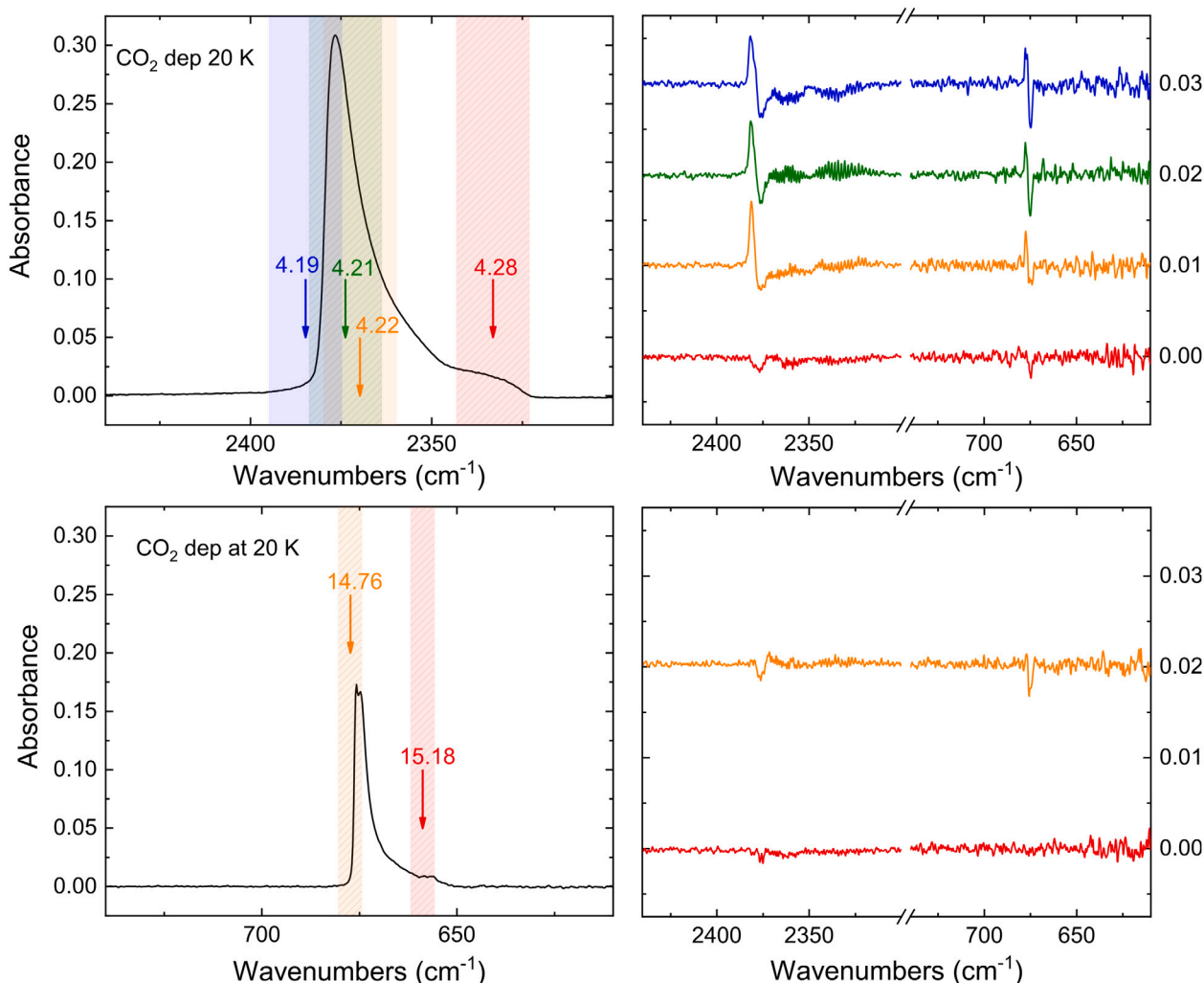
Fig. 2. FEL irradiation of pure amorphous CO_2 ice at 20 K. Left panels show an FT-RAIR spectrum of pure CO_2 ice after deposition in the ν_3 and ν_2 spectral ranges (upper and lower panels, respectively). Colored arrows and strips indicate the frequencies and FWHM of FELIX-2 used during irradiation, respectively. Right panels show FT-RAIR difference spectra before and after FEL exposure. Spectra and FEL irradiation frequencies are color-coded. Difference spectra are offset for clarity.

configuration used for the experiments presented here is such that the FEL radiation is p-polarized, i.e. with the electric vector parallel to the incidence plane and in resonance with LO phonon modes.

FEL irradiations at the CO_2 bending mode (14.76 and 15.18 μm, lower-left panel of Fig. 2) provoke spectral changes that are comparable to those seen upon irradiating ν_3 at its red wing, namely, negative peaks. Differences in spectral changes upon FEL radiation of the ν_2 and ν_3 bands suggest that on-resonance injection of vibrational energy into the CO_2 ice is a frequency dependent process. As in the case of the ν_3 band, the effect is relatively stronger for FEL irradiation at the LO phonon mode peak of the ν_2 mode and weaker at its red wing (i.e., TO phonon mode). Much like in the case of pASW, FEL irradiations performed at frequencies where the ice molecules do not present any vibrational absorption do not cause any change in the ice structure nor its thickness [15]. Hence, the difference spectra acquired before and after FEL exposure at non-resonant frequencies appear flat (spectra not shown in Fig. 2). This is a further confirmation that it is the ice that absorbs vibrational energy and not the gold substrate underneath.

To understand whether FEL radiation effects cause a global heating of the ice or not, we have compared FEL irradiations at 4.19 and 14.76 μm (left and right panels of Fig. 3, respectively) and fitted their profiles with selected FT-RAIR spectra of pure CO_2 ice deposited at 20 K and then heated during a TPD with a ramp of 2.5 K min^{-1} (see Table 1). Each panel shows an independent fit with two spectral components,

namely, a cold negative contribution at 20 K and a warm positive component at 80 K, which provided the best qualitative fits. The spectral component at 80 K shows that the ice in the control experiment has undergone restructuring during TPD toward a more crystalline-like form. The fact that a more crystalline ice (warm component) gives a positive contribution, while the amorphous ice (cold component) is a negative contribution to the fit suggests that there is a loss in amorphous ice because the ice structure reorganizes toward a more ordered configuration upon FEL exposure. Particularly, the fit at the ν_3 mode of the ice irradiated at 4.19 μm shows a 2% overall loss of column density of amorphous ice and a comparable increase in the column density of reorganized, crystalline-like, ice. When these numbers are scaled to the FEL exposed ice area on the substrate, morphological changes occur in ~50% of the irradiated molecules. Moreover, although the fit of the FEL irradiation at the ν_3 mode (4.19 μm) seems to qualitatively well reproduce the stretching mode region, changes at the ν_2 mode are not satisfactorily reproduced by the same fit. Furthermore, the FEL irradiation at the ν_2 mode (14.76 μm) cannot be reproduced by any combination of all available FT-RAIR spectra acquired during the TPD control experiment as listed in Table 1. This is because losses at the ν_2 mode due to irradiation are always larger relative to the ν_3 mode than in the case of global heating. Hence, changes in the ice induced by the FEL radiation are frequency dependent and cannot be simply explained by global thermal heating of the ice or global desorption.
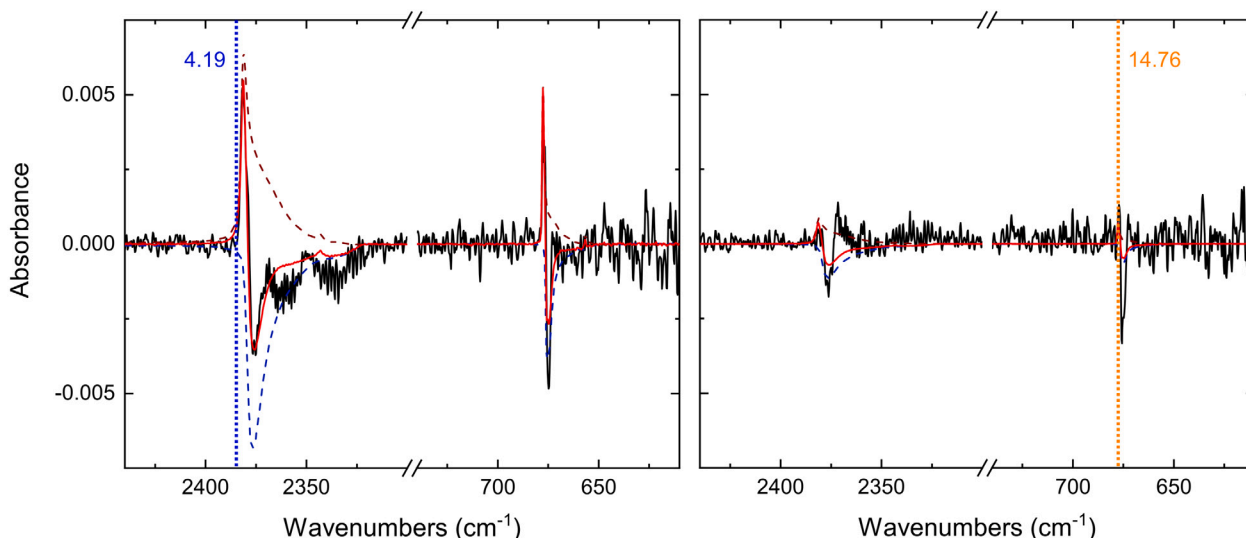
Fig. 3. Spectral fits (red solid lines) of two distinct FEL irradiations at the stretching (left panel) and bending (right panel) modes of amorphous CO_2 ice at 20 K. FT-RAIR difference spectra acquired before and after FEL exposure are presented as solid black lines. Vertical blue and orange dotted lines indicate the selected FEL radiation frequencies. The dashed red line is a FT-RAIR spectrum acquired during the TPD of an unirradiated ice at 80 K, whereas the dashed blue line is a FT-RAIR spectrum acquired at 20 K. Both spectra are used as fit components.
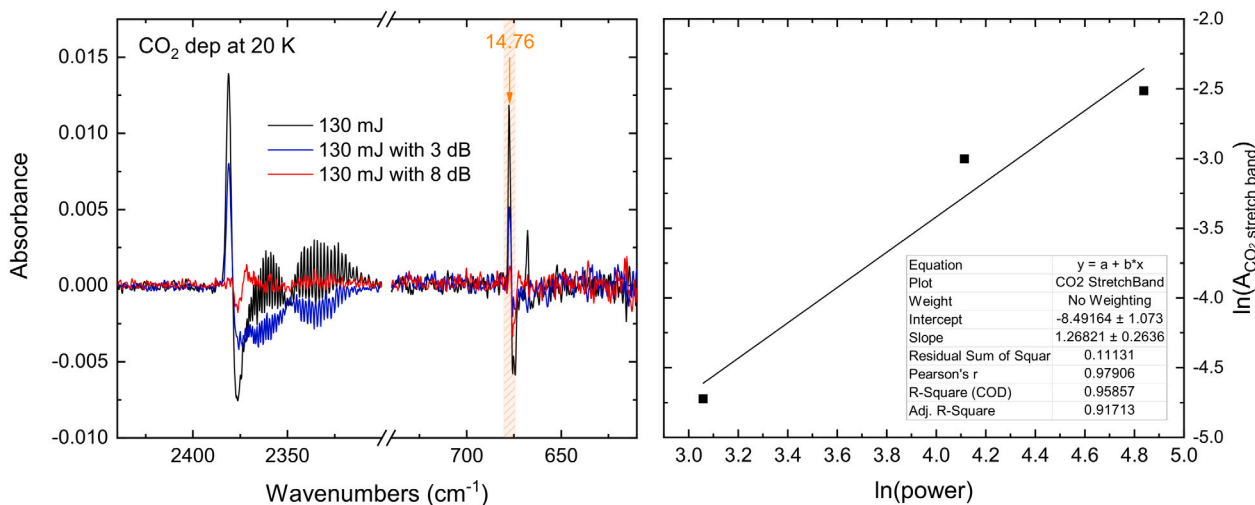

Fig. 4. Power dependence of FEL radiation and spectral changes of amorphous CO_2 ice. Left panel: in solid black, blue, and red lines, FT-RAIR difference spectra acquired before and after FEL exposure of fresh spots of CO_2 ice with 0, 3, and 8 dB attenuation, respectively. Right panel: linear fit (solid black line) of the integrated areas (black full squares) of the three FT-RAIR spectra as a function of the FEL beam power. Both axes of the right panel are on a natural logarithmic scale.

Based on our previous results in similar studies, the most likely scenario is a selective vibrational excitation, that is a local increase in vibrational energy equivalent to local heating, and possibly minor desorption of specific molecules excited by the FEL radiation at the surface and/or within the bulk of the ice. FEL irradiation at the ν_3 mode seems to induce mainly restructuring effects as shown by a combination of new positive and negative peaks in the difference spectra before and after FEL exposure, whereas irradiations at the ν_2 mode seems to lead to an additional process, wherein a vibrational selectivity gives rise to the observation of only negative peaks [42]. FEL-induced photodesorption could contribute to the observed reduction in the ν_2-mode intensity upon irradiation. However, we should not exclude other possibilities such as hole-burning effects, particularly at the irradiated frequencies. Here, QMS data is key to directly detect FEL-induced photodesorption of CO_2. Unfortunately, although QMS data were successfully recorded during ice deposition and TPD experiments, during FEL irradiation, the acquisition speed of the instrument was not optimized for the detection of gas desorption plumes ejected from the ice in short bursts due to the

pulsed nature of the FEL. Hence, during FEL irradiation, QMS results were inconclusive. The issue is beyond the scope of this paper and it will be addressed in future work.

As for the case of pASW [15], all morphological changes in the CO_2 ice are localized within the area exposed to the laser beam and do not cause a global effect throughout the ice. This is verified by acquiring FT-RAIR spectra of the ice in regions in close proximity to irradiated areas and observing no FEL radiation effects. Moreover, to test whether in this case morphological changes in the ice are due to a single-photon process, we performed a FEL power dependence study on the irradiation of the CO_2 bending mode and measured changes at both the ν_3 and ν_2 modes. The left panel of Fig. 4 shows FT-RAIR difference spectra acquired before and after FEL exposure of three fresh ice spots at three different FEL beam power settings controlled by attenuating the beam power with 0, 3, and 8 dB, corresponding to powers of 130, 65, and 20 mJ as measured by a powermeter at the FELIX control station. The right panel of Fig. 4 shows that spectral changes measured by integrating the region around the ν_3 mode are nearly linearly proportional to the
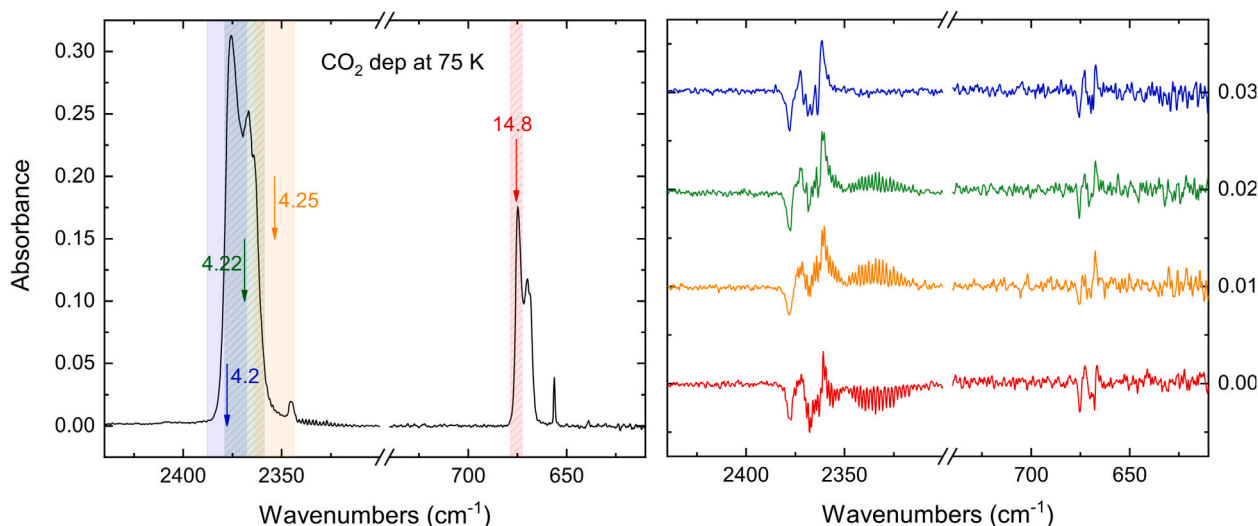
Fig. 5. FEL irradiation of pure crystalline CO_2 ice deposited at 75 K and cooled to 20 K. Left panel shows a FT-RAIR spectrum of pure CO_2 ice after deposition in the v_3 and v_2 spectral ranges. Colored arrows and strips indicate the frequencies and FWHM of FELIX-2 used during irradiation, respectively. Right panel shows FT-RAIR difference spectra before and after FEL exposure. Spectra and FEL irradiation frequencies are color-coded. Difference spectra are offset for clarity.

increase in FEL power, in agreement with the hypothesis that changes in the ice are caused by a single-photon process. However, since local temperature at the irradiated ice spot cannot be measured, we cannot completely rule-out a contribution to the changes in ice morphology being caused by laser-induced global thermal heating. However, our FT-RAIR data show that full ice desorption, hole burning and ice melting effects do not occur at the FEL exposed spot of the deposited CO_2 layer as the spectral changes observed in our experiments reveal an IR photon-induced process that is selective and frequency dependent. This is also confirmed in preliminary experiments with more volatile species, such as CO and N_2, that are more sensitive to thermal changes in the ice than CO_2. Hence, our data indicate that thermal heating is a local process and vibrational energy dissipation likely affects only a few species in the ice per impinging IR photon. Future theoretical work on molecular dynamics simulations of our experiments will provide further insights on the IR photon-induced processing of space relevant ices.

3.2. FEL irradiation of CO_2 ice deposited at 75 K

The left panel of Fig. 5 shows a FT-RAIR spectrum of pure CO_2 ice deposited at 75 K and then cooled to 20 K in both the v_3 and v_2 spectral ranges. Colored arrows indicate the frequencies at which the ice has been exposed to FELIX-2 radiation for five minutes of continuous exposure at a time and always on fresh ice spots. Vertical color-coded strips indicate the spectral FWHM of the FELIX beam at each selected wavelength. As in Fig. 2, the color of the arrows in the left panel of Fig. 5 corresponds to the color of the FT-RAIR difference spectra acquired before and after FEL exposure as shown in the right panel of the same figure. Spectral changes highlighted in the difference spectra of the right panel of Fig. 5 are all qualitatively comparable regardless of whether the ice is irradiated at the v_3 or v_2 mode. This suggests that reorganization of the ice is unlikely to occur, which was expected since the ice is already crystalline due to its deposition temperature of 75 K.

Fig. 6 shows the FT-RAIR difference spectrum of the pure CO_2 ice deposited at 75 K and then cooled to 20 K before and after being exposed to FEL radiation at 4.2 μm. The profile of the difference spectrum is fitted with two spectral components, namely, a cold negative contribution of the same ice before FEL irradiation at 20 K and a warm positive contribution of the ice as deposited at 75 K. Unlike the case of amorphous CO_2 ice, which is a metastable material, in the case of crystalline CO_2 ice, changes in the spectral profile at different

temperatures are reversible and can be obtained during multiple temperature cycles. As the cryostat cools the ice sample after deposition of a crystalline ice, IR features generally become sharper and more intense at lower temperatures (10–20 K) relative to the same features at higher temperatures (e.g., 75 K in the case of CO_2) because cooling the sample will reduce the thermal population of hot-band states of the vibrations. Such reversible process is also seen in the THz spectral range [31,43]. The lowering of the temperature reduces the thermal agitation of the lattice and consequently the phonon population in the THz range, which lowers the number of nearly equivalent classes of oscillators. This allows for a better minimization of the local potential energy.

It is worth noting that the two crystalline spectral components acquired at different temperatures of the same deposited ice prior to FEL exposure can partially fit the changes seen in the crystalline ice after FEL irradiation. However, as opposed to the case of amorphous ice seen in Fig. 2, spectral changes upon FEL exposure of crystalline CO_2 ice seem to be less dependent on the selected absorption mode. A closer look at the fit of Fig. 6 suggests that some negative peaks in both the v_3 and v_2 modes are never reproduced by the chosen fit components, indicating that some other processes such as desorption may be occurring in the ice. Here, the loss in the v_3 mode is larger than that in the v_2 band, as expected if the ice desorbed. FEL photoinduced desorption was already observed in the case of crystalline H_2O ice [11,15]. As mentioned before, QMS data are not conclusive concerning the detection of IR photodesorption. Nevertheless, indirect evidence is shown in the FT-RAIR difference spectra for both amorphous and crystalline CO_2 ice. Dedicated studies of infrared-induced photodesorption of solid molecules will be the focus of future research campaigns at HFML-FELIX Laboratory.

The difference in behavior of the pure CO_2 ices – that deposited at 20 K and that at 75 K and then cooled to 20 K – upon FEL irradiation of selected absorption vibrational modes in the MIR is new, independent evidence that CO_2 ice deposited at 20 K under our experimental conditions is an amorphous material, because it undergoes reorganization and minor desorption, whereas crystalline CO_2 ice does not show any clear sign of restructuring but mainly desorption. McGuire et al. [33] conducted a thorough investigation of the THz features of amorphous and crystalline CO_2 ice, finding unambiguous evidence that the only two features of CO_2 ice in the far-IR at 3.3 and 2.1 THz are due solely to crystalline CO_2, and that amorphous CO_2 is featureless. Our work confirms that a background slow deposition of CO_2 molecules under
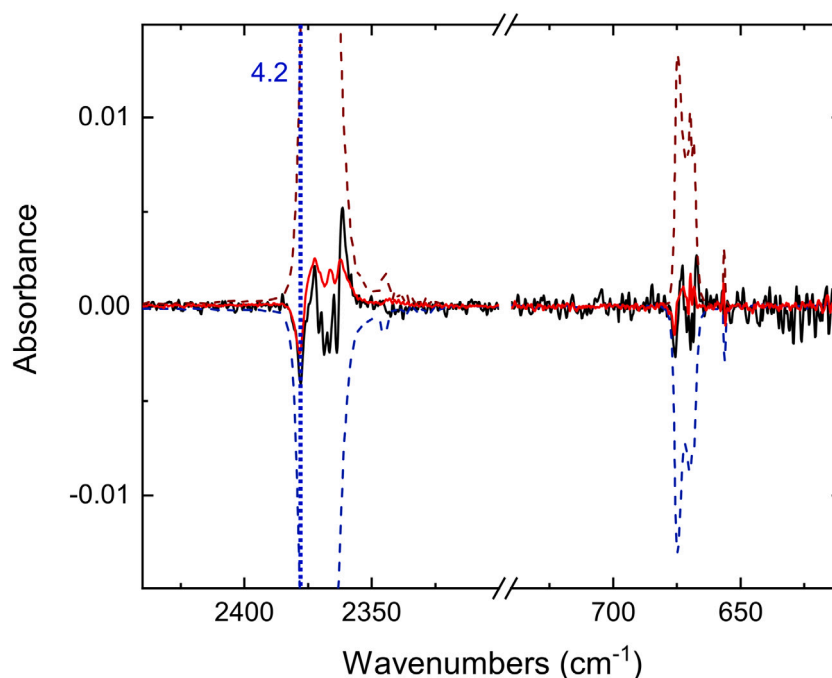
Fig. 6. Spectral fit (red solid line) of a FEL irradiation at the stretching mode of crystalline CO_2 ice deposited at 75 K and cooled to 20 K. A FT-RAIR difference spectrum acquired before and after FEL exposure is reported as a solid black line. Vertical blue dotted line indicates the selected FEL radiation frequency. Dashed red line is a FT-RAIR spectrum acquired after deposition of the ice at 75 K, whereas the dashed blue line is a FT-RAIR spectrum acquired after the ice is cooled to 20 K. Both spectra are used as fit components.

UHV conditions leads to the formation of amorphous CO_2 ice. However, we cannot rule-out that solid CO_2 samples grown under different conditions at low temperature, for instance, through direct deposition (*i.e.*, normal to the substrate face) and at higher deposition rates, may lead to the formation of the polycrystalline form of ice already reported in literature [30,32,34–36]. A further systematic investigation of different deposition conditions and ice thicknesses is needed to clarify this point.

4. Conclusions

This study focuses on the selective MIR irradiation of pure CO_2 ices deposited at 20 K and at 75 K then cooled to 20 K by means of the intense, tunable radiation of the FELIX-2 free-electron laser at the HFML-FELIX Laboratory. Experiments are carried out using the LISA end station, where ice samples are grown and monitored *in situ* by Fourier Transform Reflection–Absorption Infrared spectroscopy in the MIR range and by quadrupole mass spectrometry. We have shown that amorphous CO_2 ice goes through a restructuring process reorienting some of its molecules into a more ordered structure upon resonant absorption of IR radiation. The exposure of crystalline CO_2 ice to FEL radiation induces mostly desorption, while frequency-dependent restructuring of the ice material is not clearly observed. This work adds to the current debate on the nature of CO_2 ice in laboratory experiments and in space.

CRediT authorship contribution statement

Sergio Ioppolo: Initiated and managed the project (FELIX-2020-01-51) at HFML-FELIX Laboratory, Writing – original draft, Laboratory experiments, Data interpretation, Commented on the paper. **Jennifer A. Noble:** Supervision, Laboratory experiments, Data interpretation, Commented on the paper. **Alejandra Traspas Muiña:** Assisted during assembling and testing of the LISA end station and performed control experiments for the project, Data interpretation, Commented on the paper. **Herma M. Cuppen:** Supervision, Data interpretation, Commented on the paper. **Stéphane Coussan:** Performed some preliminary experiments, Data interpretation, Commented on the paper. **Britta Redlich:** Supervision, Data interpretation, Commented on the paper.

Declaration of competing interest

The authors declare that they have no known competing financial interests or personal relationships that could have appeared to influence the work reported in this paper.

Acknowledgments

Appendix A. Supplementary data

Supplementary material related to this article can be found online at https://doi.org/10.1016/j.jms.2022.111601.

References

[1] B.A. McGuire, 2021 Census of interstellar, circumstellar, extragalactic, protoplanetary disk, and exoplanetary molecules, Astrophys. J. 259 (2) (2021) 30, http://dx.doi.org/10.3847/1538-4365/ac2a48.

[2] E. Herbst, E.F. van Dishoeck, Complex organic interstellar molecules, Annu. Rev. Astron. Astrophys. 47 (1) (2009) 427–480, http://dx.doi.org/10.1146/annurev-astro-082708-101654.

[3] K.I. Öberg, E.A. Bergin, Astrochemistry and compositions of planetary systems, Phys. Rep. 893 (2021) 1–48, http://dx.doi.org/10.1016/j.physrep.2020.09.004, arXiv:2010.03529.

[4] S. Ioppolo, G. Fedoseev, K.J. Chuang, H.M. Cuppen, A.R. Clements, M. Jin, R.T. Garrod, D. Qasim, V. Kofman, E.F. van Dishoeck, H. Linnartz, A non-energetic mechanism for glycine formation in the interstellar medium, Nat. Astron. 5 (2021) 197–205, http://dx.doi.org/10.1038/s41550-020-01249-0, arXiv:2011.06145.

[5] E.M. Penteado, A.C.A. Boogert, K.M. Pontoppidan, S. Ioppolo, G.A. Blake, H.M. Cuppen, Spectroscopic constraints on CH_3OH formation: CO mixed with CH_3OH ices towards young stellar objects, Mon. Not. R. Astron. Soc. 454 (1) (2015) 531–540, http://dx.doi.org/10.1093/mnras/stv1987.

[6] A.C.A. Boogert, P.A. Gerakines, D.C.B. Whittet, Observations of the icy universe, Annu. Rev. Astron. Astrophys. 53 (2015) 541–581, http://dx.doi.org/10.1146/annurev-astro-082214-122348, arXiv:1501.05317.

[7] A.V. Ivlev, T.B. Röcker, A. Vasyunin, P. Caselli, Impulsive spot heating and thermal explosion of interstellar grains revisited, Astrophys. J. 805 (1) (2015) 59, http://dx.doi.org/10.1088/0004-637X/805/1/59, arXiv:1503.05012.

[8] M. Dell'Angela, T. Anniyev, M. Beye, R. Coffee, A. Föhlisch, J. Gladh, T. Katayama, S. Kaya, O. Krupin, J. LaRue, A. Møgelhøj, D. Nordlund, J.K. Nørskov, H. Öberg, H. Ogasawara, H. Öström, L.G.M. Pettersson, W.F. Schlotter, J.A. Sellberg, F. Sorgenfrei, J.J. Turner, M. Wolf, W. Wurth, A. Nilsson, Real-time observation of surface bond breaking with an X-ray laser, Science 339 (6125) (2013) 1302–1305, http://dx.doi.org/10.1126/science.1231711.

[9] H. Öström, H. Öberg, H. Xin, J. LaRue, M. Beye, M. Dell'Angela, J. Gladh, M.L. Ng, J.A. Sellberg, S. Kaya, G. Mercurio, D. Nordlund, M. Hantschmann, F. Hieke, D. Kühn, W.F. Schlotter, G.L. Dakovski, J.J. Turner, M.P. Minitti, A. Mitra, S.P. Moeller, A. Föhlisch, M. Wolf, W. Wurth, M. Persson, J.K. Nørskov, F. Abild-Pedersen, H. Ogasawara, L.G.M. Pettersson, A. Nilsson, Probing the transition state region in catalytic CO oxidation on Ru, Science 347 (6225) (2015) 978–982, http://dx.doi.org/10.1126/science.1261747.

[10] A. Krasnopoler, S.M. George, Infrared resonant desorption of H2O from ice multilayers, J. Phys. Chem. B 102 (5) (1998) 788–794, http://dx.doi.org/10.1021/jp972016q, arXiv:https://doi.org/10.1021/jp972016q.

[11] C. Focsa, B. Chazallon, J.L. Destombes, Resonant desorption of ice with a tunable LiNbO$_3$ optical parametric oscillator, Surf. Sci. 528 (1) (2003) 189–195, http://dx.doi.org/10.1016/S0039-6028(02)02631-6.

[12] J.A. Noble, C. Martin, H.J. Fraser, P. Roubin, S. Coussan, IR selective irradiations of amorphous solid water dangling modes: Irradiation vs annealing effects, J. Phys. Chem. C 118 (35) (2014) 20488–20495, http://dx.doi.org/10.1021/jp506943k, arXiv:https://doi.org/10.1021/jp506943k.

[13] J.A. Noble, C. Martin, H.J. Fraser, P. Roubin, S. Coussan, Unveiling the surface structure of amorphous solid water via selective infrared irradiation of OH stretching modes, J. Phys. Chem. Lett. 5 (5) (2014) 826–829, http://dx.doi.org/10.1021/jz5000066, PMID: 26274073. arXiv:https://doi.org/10.1021/jz5000066.

[14] S. Coussan, P. Roubin, J.A. Noble, Inhomogeneity of the amorphous solid water dangling bonds, Phys. Chem. Chem. Phys. 17 (2015) 9429–9435, http://dx.doi.org/10.1039/C5CP00662G.

[15] J.A. Noble, H.M. Cuppen, S. Coussan, B. Redlich, S. Ioppolo, Infrared resonant vibrationally induced restructuring of amorphous solid water, J. Phys. Chem. C 124 (2020) 20864–20873, http://dx.doi.org/10.1021/acs.jpcc.0c04463.

[16] H.J. Fraser, M.P. Collings, M.R.S. McCoustra, D.A. Williams, Thermal desorption of water ice in the interstellar medium, Mon. Not. R. Astron. Soc. 327 (4) (2001) 1165–1172, http://dx.doi.org/10.1046/j.1365-8711.2001.04835.x, arXiv:astro-ph/0107487.

[17] T.P.M. Goumans, M.A. Uppal, W.A. Brown, Formation of CO_2 on a carbonaceous surface: a quantum chemical study, Mon. Not. R. Astron. Soc. 384 (3) (2008) 1158–1164, http://dx.doi.org/10.1111/j.1365-2966.2007.12788.x.

[18] Y. Oba, N. Watanabe, A. Kouchi, T. Hama, V. Pirronello, Experimental study of CO_2 formation by surface reactions of non-energetic OH radicals with CO molecules, Astrophys. J. Lett. 712 (2) (2010) L174–L178, http://dx.doi.org/10.1088/2041-8205/712/2/L174.

[19] S. Ioppolo, Y. van Boheemen, H.M. Cuppen, E.F. van Dishoeck, H. Linnartz, Surface formation of CO_2 ice at low temperatures, Mon. Not. R. Astron. Soc. 413 (3) (2011) 2281–2287, http://dx.doi.org/10.1111/j.1365-2966.2011.18306.x.

[20] J.A. Noble, F. Dulieu, E. Congiu, H.J. Fraser, CO_2 formation in quiescent clouds: An experimental study of the CO + OH pathway, Astrophys. J. 735 (2) (2011) 121, http://dx.doi.org/10.1088/0004-637X/735/2/121, arXiv:1104.0031.

[21] M.H. Moore, R. Khanna, B. Donn, Studies of proton irradiated H_2O+CO_2 and H_2O+CO ices and analysis of synthesized molecules, J. Geophys. Res. 96 (E2) (1991) 17541–17545, http://dx.doi.org/10.1029/91JE01682.

[22] V. Mennella, M.E. Palumbo, G.A. Baratta, Formation of CO and CO_2 molecules by ion irradiation of water ice-covered hydrogenated carbon grains, Astrophys. J. 615 (2) (2004) 1073–1080, http://dx.doi.org/10.1086/424685.

[23] V. Mennella, G.A. Baratta, M.E. Palumbo, E.A. Bergin, Synthesis of CO and CO_2 molecules by UV irradiation of water ice-covered hydrogenated carbon grains, Astrophys. J. 643 (2) (2006) 923–931, http://dx.doi.org/10.1086/502965.

[24] M.J. Loeffler, G.A. Baratta, M.E. Palumbo, G. Strazzulla, R.A. Baragiola, CO_2 synthesis in solid CO by Lyman-α photons and 200 keV protons, Astron. Astrophys. 435 (2) (2005) 587–594, http://dx.doi.org/10.1051/0004-6361:20042256.

[25] O. Gomis, G. Strazzulla, CO_2 production by ion irradiation of H_2O ice on top of carbonaceous materials and its relevance to the Galilean satellites, Icarus 177 (2) (2005) 570–576, http://dx.doi.org/10.1016/j.icarus.2005.04.003.

[26] S. Ioppolo, M.E. Palumbo, G.A. Baratta, V. Mennella, Formation of interstellar solid CO{_2} after energetic processing of icy grain mantles, Astron. Astrophys. 493 (3) (2009) 1017–1028, http://dx.doi.org/10.1051/0004-6361:200809769.

[27] S. Ioppolo, I. Sangiorgio, G.A. Baratta, M.E. Palumbo, Solid CO_2 in low-mass young stellar objects. Comparison between spitzer and laboratory spectra, Astron. Astrophys. 554 (2013) A34, http://dx.doi.org/10.1051/0004-6361/201321176.

[28] T. Suhasaria, G.A. Baratta, S. Ioppolo, H. Zacharias, M.E. Palumbo, Solid CO_2 in quiescent dense molecular clouds. Comparison between spitzer and laboratory spectra, Astron. Astrophys. 608 (2017) A12, http://dx.doi.org/10.1051/0004-6361/201730504.

[29] C.R. Arumainayagam, R.T. Garrod, M.C. Boyer, A.K. Hay, S.T. Bao, J.S. Campbell, J. Wang, C.M. Nowak, M.R. Arumainayagam, P.J. Hodge, Extraterrestrial prebiotic molecules: photochemistry vs. radiation chemistry of interstellar ices, Chem. Soc. Rev. 48 (2019) 2293–2314, http://dx.doi.org/10.1039/C7CS00443E.

[30] R.M. Escribano, G.M. Munoz Caro, G.A. Cruz-Diaz, Y. Rodriguez-Lazcano, B. Mate, Crystallization of CO2 ice and the absence of amorphous CO2 ice in space, Proc. Natl. Acad. Sci. 110 (32) (2013) 12899–12904, http://dx.doi.org/10.1073/pnas.1222228110.

[31] M.A. Allodi, S. Ioppolo, M.J. Kelley, B.A. McGuire, G.A. Blake, The structure and dynamics of carbon dioxide and water containing ices investigated via THz and mid-IR spectroscopy, Phys. Chem. Chem. Phys. 16 (8) (2014) 3442, http://dx.doi.org/10.1039/C3CP53767F.

[32] P.A. Gerakines, R.L. Hudson, First infrared band strengths for amorphous CO_2, an overlooked component of interstellar ices, Astrophys. J. Lett. 808 (2) (2015) L40, http://dx.doi.org/10.1088/2041-8205/808/2/L40.

[33] B.A. McGuire, S. Ioppolo, M.A. Allodi, G.A. Blake, THz time-domain spectroscopy of mixed CO2-CH3OH interstellar ice analogs, Phys. Chem. Chem. Phys. 18 (30) (2016) 20199–20207, http://dx.doi.org/10.1039/C6CP00632A, arXiv:1606.03058.

[34] G.A. Baratta, M.E. Palumbo, The profile of the bending mode band in solid CO_2, Astron. Astrophys. 608 (2017) A81, http://dx.doi.org/10.1051/0004-6361/201730945.

[35] M. Tsuge, T. Nguyen, Y. Oba, T. Hama, A. Kouchi, N. Watanabe, UV-ray irradiation never causes amorphization of crystalline CO_2: A transmission electron microscopy study, Chem. Phys. Lett. 760 (2020) 137999, http://dx.doi.org/10.1016/j.cplett.2020.137999.

[36] A. Kouchi, M. Tsuge, T. Hama, Y. Oba, S. Okuzumi, S.-i. Sirono, M. Momose, N. Nakatani, K. Furuya, T. Shimonishi, T. Yamazaki, H. Hidaka, Y. Kimura, K.-i. Murata, K. Fujita, S. Nakatsubo, S. Tachibana, N. Watanabe, Transmission electron microscopy study of the morphology of ices composed of H_2O, CO_2, and CO on refractory grains, Astrophys. J. 918 (2) (2021) 45, http://dx.doi.org/10.3847/1538-4357/ac0ae6, arXiv:2109.03404.

[37] H. Yamada, W.B. Person, Absolute infrared intensities of the fundamental absorption bands in solid CO_2 and N_2O, J. Chem. Phys. 41 (8) (1964) 2478–2487, http://dx.doi.org/10.1063/1.1726291.

[38] P.A. Gerakines, W.A. Schutte, J.M. Greenberg, E.F. van Dishoeck, The infrared band strengths of H_2O, CO and CO_2 in laboratory simulations of astrophysical ice mixtures, Astron. Astrophys. 296 (1995) 810, arXiv:astro-ph/9409076.

[39] M.J. Loeffler, M.H. Moore, P.A. Gerakines, The effects of experimental conditions on the refractive index and density of low-temperature ices: Solid carbon dioxide, Astrophys. J. 827 (2) (2016) 98, http://dx.doi.org/10.3847/0004-637X/827/2/98.

[40] G.A. Baratta, M.E. Palumbo, Infrared optical constants of CO and CO_2 thin icy films, J. Opt. Soc. Amer. A 15 (12) (1998) 3076–3085, http://dx.doi.org/10.1364/JOSAA.15.003076.

[41] I.R. Cooke, E.C. Fayolle, K.I. Öberg, CO2 infrared phonon modes in interstellar ice mixtures, Astrophys. J. 832 (1) (2016) 5, http://dx.doi.org/10.3847/0004-637X/832/1/5, arXiv:1610.00294.

[42] J.S. Shirk, C.L. Marquardt, Vibrational selectivity in the single-photon infrared photochemistry of matrix-isolated 2-fluoroethanol, J. Chem. Phys. 92 (12) (1990) 7234–7240, http://dx.doi.org/10.1063/1.458209, arXiv:https://doi.org/10.1063/1.458209.

[43] S. Ioppolo, B.A. McGuire, M.A. Allodi, G.A. Blake, THz and mid-IR spectroscopy of interstellar ice analogs: methyl and carboxylic acid groups, Faraday Discuss. 168 (2014) 461, http://dx.doi.org/10.1039/C3FD00154G.